Emergence of tunable periodic density correlations in a Floquet–Bloch system

Nathan Dupont, Lucas Gabardos, Floriane Arrouas, Gabriel Chatelain, Maxime Arnal, Juliette Billy, Peter Schlagheck, B Peaudecerf, David Guéry-Odelin

PNAS RESEARCH ARTICLE | PHYSICS

Emergence of tunable periodic density correlations in a Floquet–Bloch system

Nathan Dupont[a], Lucas Gabardos[a], Floriane Arrouas[a], Gabriel Chatelain[a], Maxime Arnal[a], Juliette Billy[a], Peter Schlagheck[b], Bruno Peaudecerf[a], and David Guéry-Odelin[a,1]

Edited by William Phillips, National Institute of Standards and Technology, Gaithersburg, MD; received January 17, 2023; accepted June 16, 2023

In quantum gases, two-body interactions are responsible for a variety of instabilities that depend on the characteristics of both trapping and interactions. These instabilities can lead to the appearance of new structures or patterns. We report on the Floquet engineering of such a parametric instability, on a Bose–Einstein condensate held in a time-modulated optical lattice. The modulation triggers a destabilization of the condensate into a state exhibiting a density modulation with a new spatial periodicity. This new crystal-like order, which shares characteristic correlation properties with a supersolid, directly depends on the modulation parameters: The interplay between the Floquet spectrum and interactions generates narrow and adjustable instability regions, leading to the growth, from quantum or thermal fluctuations, of modes with a density modulation noncommensurate with the lattice spacing. This study demonstrates the production of metastable exotic states of matter through Floquet engineering and paves the way for further studies of dissipation in the resulting phase and of similar phenomena in other geometries.

cold gases in optical lattices | Floquet engineering | parametric instability

Significance

Pattern formation is a ubiquitous phenomenon in nature, from the organization of stellar nebulae to the structuration of clouds or the growth of plants. A key mechanism through which order can emerge from a homogeneous system is a parametric instability, with a paradigmatic example being the formation of Faraday waves at the surface of a vibrating liquid. Similar phenomena can occur in quantum matter, driven by interactions. Here, we demonstrate, using a Bose–Einstein condensate held in a shaken optical lattice, the emergence of an additional coherent crystal-like order with a periodic density pattern, whose spatial period directly depends on the modulation parameters. We systematically investigate this tunable order and study its growth dynamics, persistence, and decay.

The introduction of interactions in wave theory leads, through nonlinearities, to a rich phenomenology. In quantum gases, it is at the root of the modification of the equilibrium momentum distribution through the production of momentum-correlated pairs (1–4). It can also lead to instabilities that are responsible for a new structuration of the gas and the appearance of patterns. Such pattern formation may occur in static systems or through parameter quenching, which has led to the realization of spin (5) or density (6) wave patterns, or the study of supersolid order in BECs with spin–orbit coupling (7), cavity mediated (8), or dipolar interactions (9–13). It can also originate from parametric modulation, either of the trapping potential—which can lead to the formation of waves (14, 15), vortices (16, 17), or arrays (18)—or the modulation of the interaction strength (19–22).

The use of periodic parameter modulation to tailor the behavior of a quantum system lies at the heart of the broader and expanding field of Floquet engineering (23–26), where this modulation leads to effective Hamiltonians for the stroboscopic evolution. With ultracold atoms, this approach has allowed to investigate a wide range of phenomena from effective dispersion relations (27–30) to phase transitions (31–35) and to the engineering of frustrated magnetism, artificial magnetic fields, and topological bands (36–38). In the context of Floquet engineering, parametric instabilities are a subject of particular interest, both as a potential source of instability, heating, and loss of coherence (39–45) and as a way to direct pattern formation that may be used to reach specific quantum states (21, 46–48).

In this work, we exploit the tunability afforded by a Floquet system consisting of a Bose–Einstein condensate in a shaken 1D optical lattice, to control the appearance of a new, crystal-like order in the system through a parametric instability. The state produced is characterized by preserved coherence and a modulation of the density at a new spatial scale, spontaneously breaking the symmetry of the lattice, associated with the population of narrow, opposite, peaks in the momentum distribution. This is achieved through a lattice position modulation, resonant with interband transitions between initially empty modes of the ground band and an excited band. A Bogolubov analysis of the resulting effective system exhibits narrow instabilities in momentum space at opposite momenta, in the vicinity of avoided band crossings. This leads to the exponential growth, from fluctuations (which may be of quantum or thermal origin) of the population in modes with a narrow symmetrical momentum distribution. The position of these momentum components (and therefore the period of the new spatial order in the system) is tunable through a change of the modulation parameters. The resulting state is only metastable,

Author contributions: J.B., B.P., and D.G.-O. designed research; N.D., L.G., F.A., G.C., and M.A. performed research; G.C. and M.A. have observed the first experimental evidence of the instability; P.S. conceived, developed, and performed the TW simulations; B.P. and P.S. developed the tight-binding model analysis; and P.S., B.P., and D.G.-O. wrote the paper.

The authors declare no competing interest.

This article is a PNAS Direct Submission.

[1]To whom correspondence may be addressed. Email: dgo@irsamc.ups-tlse.fr.

This article contains supporting information online at https://www.pnas.org/lookup/suppl/doi:10.1073/pnas.2300980120/-/DCSupplemental.

Published August 1, 2023.

with further heating seemingly leading to its degradation. We focus in this work on the characteristics of this metastable state, obtained in the less-explored regime of interband modulations. Of particular interest are their sharpness and their tunability: This should be contrasted with the nucleation of staggered states (49–51) where unstable modes have a fixed position and a broad momentum distribution or likewise the broader distributions observed in the case of single-band parametric instabilities (43).

Our experimental observations are supported by simulations of the many-body quantum dynamics with the truncated Wigner method, which exhibit the modulated density correlations and the matter–wave coherence of the resulting state, both of them being preserved over a significant time interval.

Results

Experimental Protocol. Our experimental study relies on a rubidium-87 Bose–Einstein condensate (BEC) machine that produces pure condensates with $5 \cdot 10^5$ atoms (unless otherwise stated) in a hybrid trap (see ref. 52 and *SI Appendix 1* for more details). The BEC is adiabatically loaded in a far-detuned one-dimensional optical lattice of spacing $d = 532$ nm resulting from the interference of two counterpropagating coherent laser beams along the x-axis. The potential experienced by the atoms reads

$$V(x, y, z, t) = -\frac{s_0}{2} E_L \cos(k_L x + \varphi(t)) + U_{hyb}(x, y, z),$$

where $k_L = 2\pi/d$, s_0 measures the lattice depth in units of $E_L = \hbar^2 k_L^2/2m$ and U_{hyb} is the 3D potential of the hybrid trap, yielding a weak harmonic confinement along the lattice axis (*SI Appendix 1*). The phase $\varphi(t) = \varphi_0 \cos(2\pi\nu t)$ is modulated at a frequency resonant with interband transitions. The atoms also experience contact interactions characterized by the scattering length a_s ($a_s \simeq 5.3$ nm).

In Fig. 1, the frequency $\nu = 30$ kHz for $s_0 \simeq 3.4$ couples the ground-state band s to the third excited band f in the vicinity of quasi-momentum $q = \pm 0.36 k_L$. The series of images shows

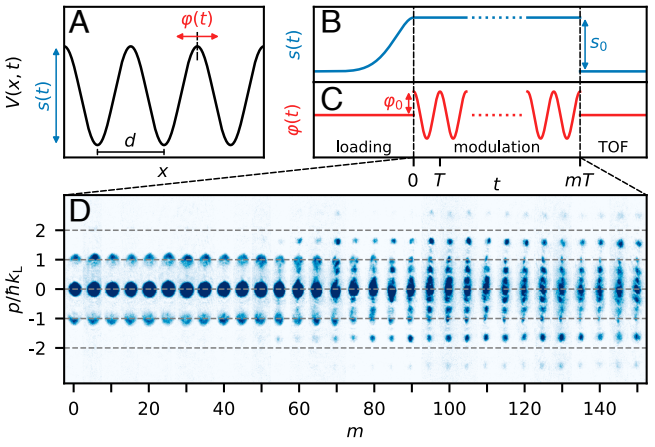

Fig. 1. Experimental protocol and typical results. (*A*) Sketch of the 1D optical lattice potential of spacing d. The depth (resp. position) of the lattice is set by the function $s(t)$ (resp. $\varphi(t)$). (*B* and *C*) Time-evolution of lattice depth (*B*) and phase (*C*), showing the adiabatic loading to the ground state of the lattice, the phase modulation experiment for an integer number of periods, and the lattice release and time of flight (TOF). (*D*) Stack of experimental absorption images after time of flight showing the stroboscopic evolution of the momentum distribution of an initial BEC with $N = 10^5$ atoms, as a function of the number m of periods of modulation T, with $s_0 = 3.40 \pm 0.10$ (here and throughout the article, given uncertainties refer to one standard deviation), $\varphi_0 = 20°$, $\nu = 1/T = 30$ kHz and $t_{TOF} = 35$ ms.

the evolution of the matter-wave diffraction pattern measured by absorption after a long time of flight ($t_{TOF} = 35$ ms). It represents the stroboscopic evolution of the atomic momentum distribution in the modulated lattice at integer multiples m of the modulation period. For short modulation times, we mostly observe three diffraction peaks centered on integer multiples of h/d and associated with the initial ground-state distribution of the static lattice. A faint halo is visible between the peaks, which originates from elastic collisions occurring during the time of flight (53–55). After 70 modulation periods ($\simeq$2.3 ms), we clearly observe the emergence of symmetric diffraction peaks located in between the ordinary diffraction peaks. The initial growth of the population in the peaks appears to settle, with the new peaks remaining sharp over many modulation periods. Over longer timescales (see below), each narrow peak eventually seems to slowly broaden.

Tight-Binding Effective Model and Tunability. We interpret the emergent momentum peaks as originating from a parametric instability favoring a four-wave mixing process in which two atoms from the BEC with $q_{in} = 0$ scatter into quasi-momenta at $q = \pm q^*$ with $0 < q^* < \pi/d$. This is associated with the emergence of a new spatial periodicity $d^* = \pi/q^*$ in the system. Correspondingly, the momentum distribution exhibits two families of peaks at momenta $p = \pm q^* + \ell k_L, \ell \in \mathbb{Z}$, related to the decomposition of the newly populated states in the band structure of the lattice potential. This interpretation and the physics at play are correctly captured by an effective tight-binding model with two coupled bands, describing the Floquet system of lattice bands coupled by the lattice shaking (*SI Appendix 2*). For realistic parameters, the Bogolubov treatment of this model reveals sharply localized unstable modes in the vicinity of the avoided band crossings. The position of the most unstable mode yields the central quasi-momenta $q = \pm q^*$. From this modeling, we infer that the position of the instability in quasi-momentum smoothly depends on the model's parameters, namely the modulation frequency ν and amplitude φ_0, as well as the strength of interactions in the initial condensate.

In Fig. 2, we compare the measured position (in terms of the reduced momentum k/k_L of the unfolded band structure) of the peaks emerging after a sufficiently long modulation time to the position of resonant transitions from the lowest band, as the frequency of modulation is varied. The modulation frequency is tuned across two bands and is resonant with s to d transitions at low frequencies ($\nu < 26.1$ kHz) and with s to f transitions at higher frequencies ($\nu > 28.3$ kHz). As expected, the instability experimentally occurs in the vicinity of the band crossing. It seems however that the instability is systematically closer to the actual band crossing experimentally than expected from the model (which predicts it to be a few percent of k_L away from the crossing). Nevertheless, this demonstrates the tunability of the instability position in quasi-momentum space. The interpretation of the instability pattern for a transition frequency near the gap between bands d and f is more involved, as there is then a possibility of a resonant excitation of the condensate.

Truncated Wigner Simulation and Correlations. To further investigate the coherence properties of the atomic state arising from the parametric instability, we perform numerical simulations of the modulated system, based on the Truncated Wigner method at zero temperature (56–59). In these simulations, the quantum state is expanded on the Wannier functions of the first five

energy bands of the static lattice over a finite size system, taking into account the external confinement U_{hyb}. This approach gives direct access to the first- and second-order correlation functions, revealing the features of the underlying many-body physics. After a sufficiently long evolution time, the spectrum of the one-body density matrix contains a dominant eigenvalue corresponding to the Bose–Einstein condensate at zero quasi-momentum, plus two other significant eigenvalues corresponding to two states with opposite parity made of opposite quasi-momenta components (*SI Appendix 4*).

The macroscopic occupation of modes having opposite quasi-momenta in the Brillouin zone raises the question of the possible emergence of a long-range order in the system. To answer this question, we exploit our beyond-mean-field calculations to compute the atom density on each site across the system. Strikingly, in Fig. 3*A*, after 5 ms of evolution, we see the evidence on individual TW trajectories of the emergence of a new periodic modulation of the density within the lowest band of the lattice, on a scale of about three lattice sites. This is related to the quasi-momentum at which the instability occurs, which is $q^*/k_{\mathrm{L}} \simeq 0.29$, leading to a spacing $d^*/d \simeq 3.4$, which is reasonably close and compatible with the experimental finding of $q^*/k_{\mathrm{L}} = 0.36 \pm 0.05$ for the same set of parameters.* In each trajectory from the TW simulation, the phase reference of the density modulation appears random, which washes out the modulation on the average density (full line in Fig. 3*A*). We can recover evidence for the modulation by computing the normalized density–density correlation function in the lowest band $g^{(2)}(\ell) = \langle n_0 n_\ell \rangle / (\langle n_0 \rangle \langle n_\ell \rangle)$, between the central site of the lattice and a site ℓ, averaged over 1,000 TW trajectories. This is plotted in Fig. 3*B* as a function of the site position ℓ. It reveals strong, regular, density oscillations across the system which signal the emergence of a new extended periodic order. Finally, in Fig. 3*C*, we similarly compute a normalized coherence within the ground band between sites 0 and ℓ in the system $g^{(1)}(\ell) = \langle \hat{a}_0^\dagger \hat{a}_\ell \rangle / (\langle n_0 \rangle \langle n_\ell \rangle)^{1/2}$. This shows modulations with a similar period, demonstrating the coexistence across the system of the initial condensate of period d as well as fully coherent states with the new period d^*. This coherence is further demonstrated by the time-of-flight diffraction pattern. The simulations show that the finite extent of the correlations grows with time, with Fig. 3 showing an intermediate stage of their development and correlations potentially extending across the whole sample with minimal decay (*SI Appendix 4*).

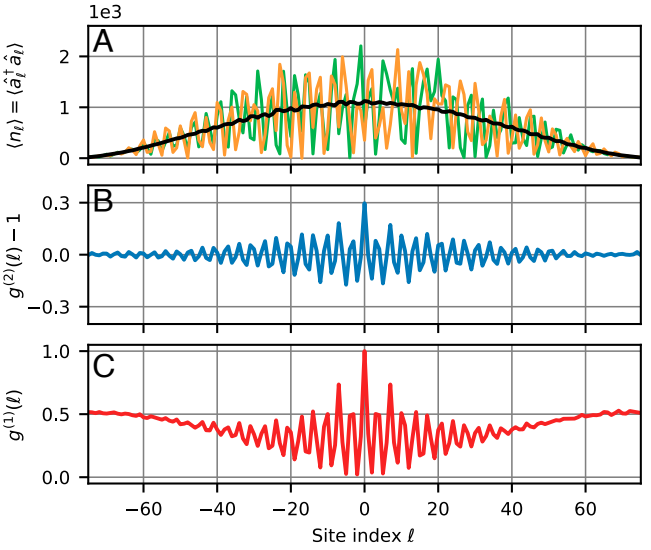

Fig. 3. Correlations and coherence after nucleation of the instability. (*A*) Density distribution in the *s* band from TW simulations of a 1D modulated lattice with realistic trapping (see text for details). The chosen lattice parameters are $s_0 = 3.4$, $\nu = 30$ kHz, and $\varphi_0 = 20°$, with a number of atoms $N = 10^5$. The density is computed after a modulation duration of 5 ms, when the instability is visible in the momentum distribution. Two individual TW trajectories (green and orange lines) exhibit a clear periodic modulation of the density, which is washed out in the average of 1,000 trajectories (thick black line). (*B* and *C*) In the same conditions as (*A*), average density correlation function $g^{(2)}(\ell)$ (*B*) and average amplitude correlation function $g^{(1)}(\ell)$ (*C*) between the central site and a site ℓ in the *s* band of the lattice potential (see text for definitions).

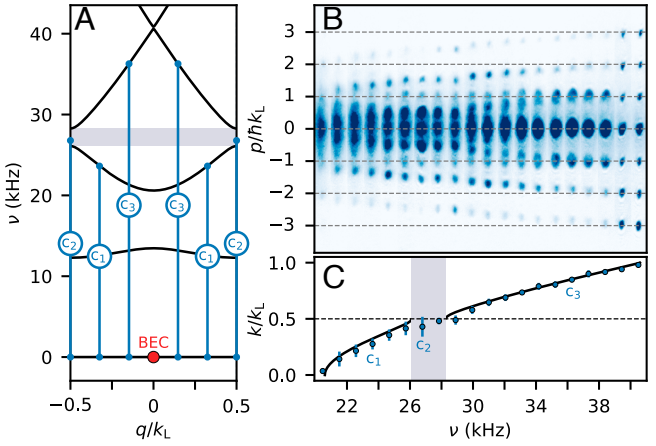

Fig. 2. Instability displacement with the modulation frequency. (*A*) Transition diagram from the lowest band *s* over the first Brillouin zone (BZ) (solid black line) and addressed transitions for data c_1, c_2, and c_3 (blue dots and solid lines) as a function of quasi-momentum q/k_{L}. The ground state of the static lattice initially populated by the BEC is denoted by a red disk. In (*A*–*C*), the gap between the transitions *s*-*d* and *s*-*f* (gray-shaded area) is represented. (*B*) Stack of experimental absorption images after $n = 100$ periods, averaged over 3 realizations, for an increasing modulation frequency ν, with $s_0 = 3.57 \pm 0.10$, $\varphi_0 = 15°$, and $t_{\mathrm{TOF}} = 35$ ms. (*C*) Average instability position (in terms of the reduced momentum k/k_{L} of the unfolded band structure) extracted from the fitted change in the position of the four $1 \leq |p|/\hbar k_{\mathrm{L}} \leq 3$ orders of diffraction over all realizations (blue dots, error bars correspond to the standard deviation of the 12-point sample) and calculated position of the resonant coupling as a function of the modulation frequency (solid black line). The position corresponding to the edge of the first BZ is denoted by a dashed line.

The appearance of these modulations is actually already present within the tight-binding model, in an estimate of the correlation functions (*SI Appendix 2*). This estimate allows us to highlight the fact that the appearance of this new spatial order is intimately related to the sharpness of the instability maximum in momentum space, which distinguishes the resulting state from staggered states (49–51). These properties of the correlation functions are reminiscent of those of a supersolid state; however, it must be emphasized that the produced state is metastable and cannot to our knowledge be characterized as the ground state of an effective Hamiltonian, thereby lacking a key property to be qualified as a supersolid.

Nucleation Timescale. The two-band tight-binding model can provide an estimate for the value of the instability exponents, and therefore, the characteristic timescale for the exponential growth of unstable modes, but it cannot provide the full dynamics of the

*Experimental uncertainties in the lattice depth s_0 can lead to a relative uncertainty on the determination of the quasi-momentum for which the frequency of the modulation drives a transition resonantly, of about 5% for these parameters.

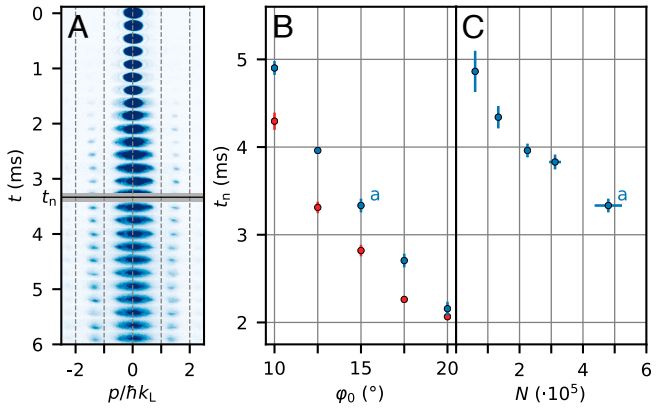

Fig. 4. Nucleation time of the instability. (*A*) Experimental record for determining the nucleation timescale: Using band-mapping before imaging leads to well-isolated contributions from higher lattice bands (here for $1 < |p|/(\hbar k_L) < 2$) signaling the growth of the instability. This growth is fitted to extract a nucleation time t_n, denoted by the horizontal line, with uncertainty represented by the shaded area (see text for details). (*B*) Evolution of the measured nucleation time of the unstable modes (see text) as a function of the modulation amplitude φ_0 for $\nu = 25.5$ kHz and $s_0 = 3.70 \pm 0.20$ (blue, coupling bands *s-d*) and $\nu = 30.5$ kHz and $s_0 = 3.56 \pm 0.20$ (red, coupling bands *s-f*). Error bars correspond to one standard deviation on the fit (see text). (*C*) Same as (*B*) as a function of the number of atoms N in the BEC for $\nu = 25.5$ kHz and $s_0 = 3.58 \pm 0.30$, for a fixed modulation amplitude $\varphi_0 = 15°$. Error bars correspond vertically to one standard deviation on the fit and horizontally to one standard deviation over four independent measurements of the atom number.

mode growth nor their subsequent evolution. However, the real timescale information can be readily accessed experimentally. In Fig. 4, we measured the nucleation time t_n as a function of the modulation amplitude φ_0 and the number of atoms N in the BEC. To precisely extract the value of t_n, we used a band-mapping technique (*SI Appendix 5*): After modulating the lattice for an integer number of modulation periods, the modulation is stopped, and the lattice depth adiabatically lowered before performing a time of flight. This technique allows us to unambiguously identify the population of modes in the excited bands at finite quasi-momenta resulting from the instability and reduces the impact of remnant collision halos on the measurement compared with a direct time-of-flight measurement. The growth of the population in the higher band modes is fitted with a sigmoid growth curve to yield a nucleation time at the half-maximum point.

Our results in Fig. 4 show that the nucleation time decreases with the modulation amplitude and the number of atoms N (experimentally, the number of atoms in the BEC can be reduced by a factor of up to ten in a reproducible manner by evaporating the BEC held in the hybrid trap before loading the lattice). These trends are similar to those observed for the single-band Bogolubov instability leading to staggered states (50). They also are expected from trends in the tight-binding model for realistic parameters (*SI Appendix 2*): By increasing the modulation amplitude φ_0, we increase the coupling between bands, which leads to larger instability exponents. The variation of the nucleation time with N is also qualitatively expected: Indeed, the initial interaction energy in the condensate increases with N and is also associated with a stronger instability. The TW simulations provide a more accurate and complete description of the evolution of the system, that should be qualitatively correct (within the approximations of the model). That is indeed the case: With the shared parameters of Figs. 1 (experiment) and 3 (simulation), the instability occurs at the same position in momentum space. The nucleation time in simulations is longer than in experiments, by about a factor of 2: This may be due to a thermal activation in the experiment (the simulations are at zero-temperature) or a contribution of the transverse degrees of freedom, that are not included in the 1D simulations.

We restricted our measurements to small values of φ_0, beyond which the validity of the two-band model and of our interpretation becomes questionable. Indeed, for stronger coupling values, the Floquet spectrum increasingly contains significant avoided crossings and fully hybridized bands, and the evolution of the system is expected to get more complex.

Discussion

We have also investigated the survival of the produced state after saturation of the instability. This is illustrated in Fig. 5. As mentioned earlier, after the population of the newly formed peaks in the momentum distribution settles (as seen from the band-mapping data), the peaks at $q = \pm q^*$ seem to slowly broaden, presumably through some further instability that leads to heating. Interestingly, this heating effect, and the eventual destruction of correlations, seems more pronounced in simulations than in experiments. In simulations, the sharp peaks at $q = \pm q^*$ only exist in a small time interval around t_n, while experimentally (Fig. 5), we can reliably see the contributions at $\pm q^*$ after nucleation over a duration of order $3t_n$. We hypothesize that this longer persistence in experiments than in numerical simulations may originate from the transverse degrees of freedom in the experimental system (absent in the simulation), which offer more possibilities for effective heat dissipation and can affect parametric instabilities (43).

In summary, we have investigated how a tunable crystal-like order with tunable periodic correlations emerges from atom–atom interactions seeded by fluctuations in a Floquet system generated by resonant band coupling. The tunable extended order observed here is synthesized and controlled by the parameters of the modulation and an atomic four-wave mixing effect stemming from contact interactions in the ultracold regime. It is as such applicable to other atomic species or systems with contact interactions. A key feature of this instability is the ability, via the coupling to higher bands, to tailor both the position and width of the instability, which adjusts the periodicity and range of first- and second-order correlations. Further investigations into this effect can be envisioned to characterize the ulterior broadening of the momentum components and the stability of the system (with the possible existence of stable regions of modulation) to

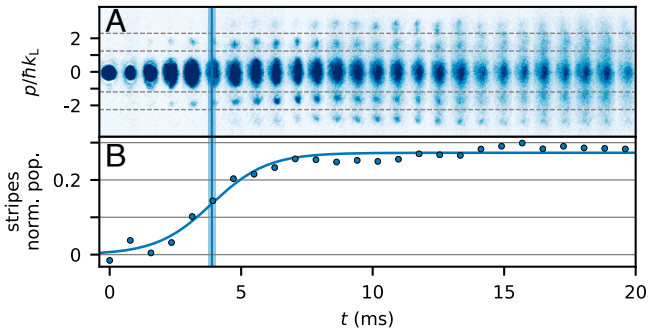

Fig. 5. Long-term survival of the emerging crystal-like order. (*A*) Experimental stroboscopic evolution of the momentum distribution after band-mapping over 510 periods of modulation. Modulation parameters are $s_0 = 3.8 \pm 0.1$, $\nu = 25.5$ kHz, and $\varphi_0 = 15°$. The initial growth of the instability is monitored by counting the relative atomic population in the two stripes delimited by dashed lines. (*B*) Evolution of the normalized population in momentum peaks created by the instability [stripes in (*A*)]. A sigmoid fit allows us to determine the nucleation timescale $t_n \simeq 4$ ms. The population in the nucleated modes then settles and remains identifiable on a timescale of several t_n, but an eventual broadening of the momentum peaks is clearly visible in (*A*).

possibly observe in situ the density modulation, for example, through the quantum gas magnifier technique (60, 61), or to explore similar effects in higher dimensions and/or other lattice geometries. This work highlights the potential of the interplay between Floquet engineering and interactions for the preparation and manipulation of exotic quantum states.

Data, Materials, and Software Availability. All study data are included in the article and/or *SI Appendix*. The data and codes supporting the findings of this study are available at https://zenodo.org/record/8127829 (62).

ACKNOWLEDGMENTS. We thank Jean Dalibard for helpful discussions. This work was supported by research funding Grant No. ANR-17-CE30-0024. N.D. and F.A. acknowledge support from Région Occitanie and Université Toulouse III-Paul Sabatier. M.A. acknowledges support from the DGA (Direction Générale de l'Armement).

Author affiliations: [a]Laboratoire Collisions Agrégats Réactivité, UMR 5589, Fédération de Recherche Matière et Interactions, Université Toulouse 3, CNRS, Toulouse, CEDEX 09 31062, France; and [b]Complex and Entangled Systems from Atoms to Materials Research Unit, University of Liège, 4000 Liège, Belgium

1. R. Lopes *et al*., Quantum depletion of a homogeneous Bose–Einstein condensate. *Phys. Rev. Lett.* **119**, 190404 (2017).
2. K. Xu *et al*., Observation of strong quantum depletion in a gaseous Bose–Einstein condensate. *Phys. Rev. Lett.* **96**, 180405 (2006).
3. H. Cayla *et al*., Hanbury Brown and Twiss bunching of phonons and of the quantum depletion in an interacting Bose gas. *Phys. Rev. Lett.* **125**, 165301 (2020).
4. A. Tenart, G. Hercé, J. P. Bureik, A. Dareau, D. Clément, Observation of pairs of atoms at opposite momenta in an equilibrium interacting Bose gas. *Nat. Phys.* **17**, 1364–1368 (2021).
5. J. Kronjäger, C. Becker, P. Soltan-Panahi, K. Bongs, K. Sengstock, Spontaneous pattern formation in an antiferromagnetic quantum gas. *Phys. Rev. Lett.* **105**, 090402 (2010).
6. C. L. Hung, V. Gurarie, C. Chin, From cosmology to cold atoms: Observation of Sakharov oscillations in a quenched atomic superfluid. *Science* **341**, 1213–1215 (2013).
7. J. R. Li *et al*., A stripe phase with supersolid properties in spin-orbit-coupled Bose–Einstein condensates. *Nature* **543**, 91–94 (2017).
8. J. Léonard, A. Morales, P. Zupancic, T. Esslinger, T. Donner, Supersolid formation in a quantum gas breaking a continuous translational symmetry. *Nature* **543**, 87–90 (2017).
9. F. Böttcher *et al*., Transient supersolid properties in an array of dipolar quantum droplets. *Phys. Rev. X* **9**, 011051 (2019).
10. L. Tanzi *et al*., Observation of a dipolar quantum gas with metastable supersolid properties. *Phys. Rev. Lett.* **122**, 130405 (2019).
11. L. Chomaz *et al*., Observation of roton mode population in a dipolar quantum gas. *Nat. Phys.* **14**, 442–446 (2018).
12. L. Chomaz *et al*., Long-lived and transient supersolid behaviors in dipolar quantum gases. *Phys. Rev. X* **9**, 021012 (2019).
13. J. Zhang, C. Zhang, J. Yang, B. Capogrosso-Sansone, Supersolid phases of lattice dipoles tilted in three dimensions. *Phys. Rev. A* **105**, 063302 (2022).
14. P. Engels, C. Atherton, M. A. Hoefer, Observation of Faraday waves in a Bose–Einstein condensate. *Phys. Rev. Lett.* **98**, 095301 (2007).
15. R. Cominotti *et al*., Observation of massless and massive collective excitations with Faraday patterns in a two-component superfluid. *Phys. Rev. Lett.* **128**, 210401 (2022).
16. K. W. Madison, F. Chevy, V. Bretin, J. Dalibard, Stationary states of a rotating Bose–Einstein condensate: Routes to vortex nucleation. *Phys. Rev. Lett.* **86**, 4443–4446 (2001).
17. S. Sinha, Y. Castin, Dynamic instability of a rotating Bose–Einstein condensate. *Phys. Rev. Lett.* **87**, 190402 (2001).
18. B. Mukherjee *et al*., Crystallization of bosonic quantum Hall states in a rotating quantum gas. *Nature* **601**, 58–62 (2022).
19. J. H. V. Nguyen, D. Luo, R. G. Hulet, Formation of matter-wave soliton trains by modulational instability. *Science* **356**, 422–426 (2017).
20. J. Nguyen *et al*., Parametric excitation of a Bose–Einstein condensate: From Faraday waves to granulation. *Phys. Rev. X* **9**, 011052 (2019).
21. Z. Zhang, K. X. Yao, L. Feng, J. Hu, C. Chin, Pattern formation in a driven Bose–Einstein condensate. *Nat. Phys.* **16**, 652–656 (2020).
22. S. Fazzini, P. Chudzinski, C. Dauer, I. Schneider, S. Eggert, Nonequilibrium Floquet steady states of time-periodic driven Luttinger liquids. *Phys. Rev. Lett.* **126**, 243401 (2021).
23. N. Goldman, J. Dalibard, Periodically driven quantum systems: Effective Hamiltonians and engineered gauge fields. *Phys. Rev. X* **4**, 031027 (2014).
24. M. Holthaus, Floquet engineering with quasienergy bands of periodically driven optical lattices. *J. Phys. B: At. Mol. Opt. Phys.* **49**, 013001 (2016).
25. A. Eckardt, Colloquium: Atomic quantum gases in periodically driven optical lattices. *Rev. Mod. Phys.* **89**, 011004 (2017).
26. C. Weitenberg, J. Simonet, Tailoring quantum gases by Floquet engineering. *Nat. Phys.* **17**, 1342–1348 (2021).
27. K. W. Madison, M. C. Fischer, R. B. Diener, Q. Niu, M. G. Raizen, Dynamical Bloch band suppression in an optical lattice. *Phys. Rev. Lett.* **81**, 5093–5096 (1998).
28. H. Lignier *et al*., Dynamical control of matter-wave tunneling in periodic potentials. *Phys. Rev. Lett.* **99**, 220403 (2007).
29. E. Kierig, U. Schnorrberger, A. Schietinger, J. Tomkovic, M. K. Oberthaler, Single-particle tunneling in strongly driven double-well potentials. *Phys. Rev. Lett.* **100**, 190405 (2008).
30. L. C. Ha, L. W. Clark, C. V. Parker, B. M. Anderson, C. Chin, Roton-Maxon excitation spectrum of Bose condensates in a shaken optical lattice. *Phys. Rev. Lett.* **114**, 055301 (2015).
31. A. Eckardt, C. Weiss, M. Holthaus, Superfluid-insulator transition in a periodically driven optical lattice. *Phys. Rev. Lett.* **95**, 260404 (2005).
32. A. Zenesini, H. Lignier, D. Ciampini, O. Morsch, E. Arimondo, Coherent control of dressed matter waves. *Phys. Rev. Lett.* **102**, 100403 (2009).
33. C. V. Parker, L. C. Ha, C. Chin, Direct observation of effective ferromagnetic domains of cold atoms in a shaken optical lattice. *Nat. Phys.* **9**, 769–774 (2013).
34. L. Feng, L. W. Clark, A. Gaj, C. Chin, Coherent inflationary dynamics for Bose–Einstein condensates crossing a quantum critical point. *Nat. Phys.* **14**, 269–272 (2018).
35. B. Song *et al*., Realizing discontinuous quantum phase transitions in a strongly correlated driven optical lattice. *Nat. Phys.* **18**, 259–264 (2022).
36. J. Struck *et al*., Quantum simulation of frustrated classical magnetism in triangular optical lattices. *Science* **333**, 996–999 (2011).
37. M. Aidelsburger *et al*., Experimental realization of strong effective magnetic fields in an optical lattice. *Phys. Rev. Lett.* **107**, 255301 (2011).
38. N. Cooper, J. Dalibard, I. Spielman, Topological bands for ultracold atoms. *Rev. Mod. Phys.* **91**, 015005 (2019).
39. S. Lellouch, M. Bukov, E. Demler, N. Goldman, Parametric instability rates in periodically driven band systems. *Phys. Rev. X* **7**, 021015 (2017).
40. M. Reitter *et al*., Interaction dependent heating and atom loss in a periodically driven optical lattice. *Phys. Rev. Lett.* **119**, 200402 (2017).
41. S. Lellouch, N. Goldman, Parametric instabilities in resonantly-driven Bose–Einstein condensates. *Quantum Sci. Technol.* **3**, 024011 (2018).
42. T. Boulier *et al*., Parametric heating in a 2D periodically driven Bosonic system: Beyond the weakly interacting regime. *Phys. Rev. X* **9**, 011047 (2019).
43. K. Wintersperger *et al*., Parametric instabilities of interacting Bosons in periodically driven 1D optical lattices. *Phys. Rev. X* **10**, 011030 (2020).
44. A. Rubio-Abadal *et al*., Floquet prethermalization in a Bose–Hubbard system. *Phys. Rev. X* **10**, 021044 (2020).
45. A. Di Carli *et al*., Instabilities of interacting matter waves in optical lattices with Floquet driving. arXiv [Preprint] (2023). http://arxiv.org/abs/2303.06092v1 (Accessed 24 April 2023).
46. G. K. Campbell *et al*., Parametric amplification of scattered atom pairs. *Phys. Rev. Lett.* **96**, 020406 (2006).
47. B. Galilo, D. K. K. Lee, R. Barnett, Selective population of edge states in a 2D topological band system. *Phys. Rev. Lett.* **115**, 245302 (2015).
48. G. Engelhardt, M. Benito, G. Platero, T. Brandes, Topological instabilities in AC-driven Bosonic systems. *Phys. Rev. Lett.* **117**, 045302 (2016).
49. N. Gemelke, E. Sarajlic, Y. Bidel, S. Hong, S. Chu, Parametric amplification of matter waves in periodically translated optical lattices. *Phys. Rev. Lett.* **95**, 170404 (2005).
50. E. Michon *et al*., Phase transition kinetics for a Bose Einstein condensate in a periodically driven band system. *New J. Phys.* **20**, 053035 (2018).
51. M. Mitchell *et al*., Floquet solitons and dynamics of periodically driven matter waves with negative effective mass. *Phys. Rev. Lett.* **127**, 243603 (2021).
52. A. Fortun *et al*., Direct tunneling delay time measurement in an optical lattice. *Phys. Rev. Lett.* **117**, 010401 (2016).
53. M. Greiner, I. Bloch, O. Mandel, T. W. Hänsch, T. Esslinger, Exploring phase coherence in a 2D lattice of Bose–Einstein condensates. *Phys. Rev. Lett.* **87**, 160405 (2001).
54. A. Tenart *et al*., Two-body collisions in the time-of-flight dynamics of lattice Bose superfluids. *Phys. Rev. Res.* **2**, 013017 (2020).
55. G. Chatelain *et al*., Observation and control of quantized scattering halos. *New J. Phys.* **22**, 123032 (2020).
56. M. J. Steel *et al*., Dynamical quantum noise in trapped Bose–Einstein condensates. *Phys. Rev. A* **58**, 4824–4835 (1998).
57. A. Sinatra, C. Lobo, Y. Castin, The truncated Wigner method for Bose-condensed gases: Limits of validity and applications. *J. Phys. B: At., Mol. Opt. Phys.* **35**, 3599–3631 (2002).
58. A. Polkovnikov, Phase space representation of quantum dynamics. *Ann. Phys.* **325**, 1790–1852 (2010).
59. J. Dujardin, T. Engl, J. D. Urbina, P. Schlagheck, Describing many-body Bosonic waveguide scattering with the truncated Wigner method. *Ann. Phys.* **527**, 629–638 (2015).
60. L. Asteria, H. P. Zahn, M. N. Kosch, K. Sengstock, C. Weitenberg, Quantum gas magnifier for sub-lattice-resolved imaging of 3D quantum systems. *Nature* **599**, 571–575 (2021).
61. H. Zahn *et al*., Formation of spontaneous density-wave patterns in DC driven lattices. *Phys. Rev. X* **12**, 021014 (2022).
62. N. Dupont *et al*., Emergence of tunable periodic density correlations in a Floquet-Bloch system. Zenodo. https://zenodo.org/record/8127829. Deposited 9 July 2023.